CFD modelling of hydroacoustic performance of marine propellers: Predicting propeller cavitation

Vladimir Krasilnikov
SINTEF Ocean, Trondheim/Norway
vladimir.krasilnikov@sintef.no

1 Challenges associated with modelling propeller hydroacoustics

According to the recent estimations, the radiated underwater noise due to shipping activities raises the natural underwater background noise level, in the frequency range from 10 to 300Hz, by 20 to 30 dB. With an increase of about 3dB per decade, this development is extremely fast in comparison with evolutionary timescales for some of the affected sea fauna to adapt. Low frequency noise covering the 63 Hz to 125 Hz 1/3 octave bands is dominated by propeller cavitation. The noise emissions in the same and higher frequency range interfere with acoustic sensors used by naval, research and oceanographic vessels and underwater monitoring systems. The analysis of full-scale measurements conducted on a variety of merchant ship types indicates that the highest levels of on-board noise are frequently noted in the same lower-frequency bands as mentioned above, and they are thus attributed to propeller cavitation. From the standpoint of numerical simulation of propeller acoustics, the major challenges are related to: 1) resolution of highly anisotropic fields of turbulence in the wake of ship hull and propeller-induced vorticity; 2) prediction of dynamic behaviour of cavitation on propeller blades and in propeller-induced vortices; 3) solution of acoustic propagation in the ambient flow domain.

While it is used successfully in self-propulsion calculations, the RANS method shows serious limitations in the resolution of hull and propeller vorticity field. Insufficient accuracy of this method is the consequence of averaging of the Navier-Stokes equations and excessive numerical diffusion caused by the assumption about isotropic pattern of turbulence employed by most of turbulence models of industrial use. While the LES approach is shown to be the most adequate platform for this type of analysis (Bensow & Liefvendahl, 2016), in practice it comes at great computation costs and reveals dependence on mesh quality and solution settings. Usually, the prediction of propeller forces by the LES method is less reliable compared to the RANS method. Therefore, hybrid solutions such as DES or embedded LES are often viewed as a viable alternative to LES to predict the hydrodynamic sources of noise, in both the non-cavitating and cavitating propeller flow scenarios (Shin & Andersen, 2018). Regarding the modelling of cavitation, the asymptotic cavitation models such as the popular model by Schnerr-Sauer are considered sufficient for capturing overall fluctuations of blade sheet cavitation caused by blade passing through a non-uniform wake. However, the dynamic processes that accompany cavity closure (vortex shedding, detached bubbly clouds) require more elaborate modelling where the effects of bubble inertia, viscous diffusion and surface tension are accounted for. This type of modelling is possible with the model based on the full Reyleigh-Plesset equation (Muzaferija et.al., 2017). Further complications arise from the interaction between the different types of cavitation, e.g. sheet and vortex cavitation which is often observed on marine propellers at the outer blade radii. As regards the numerical treatment of the said phenomena, the interaction between the turbulence modelling approach and phase change model is critical. Even with the DES method, tracking a cavitating propeller tip vortex sufficiently far downstream of propeller may be problematic. As one moves further down the propeller slipstream, the interaction between the blade tip vortices and propeller hub vortex becomes increasingly important (Felli et.al., 2014).

Pressure fluctuations in the near field around propeller can be computed directly from the CFD solution. However, under the assumption of flow incompressibility and without adequate mesh resolution, sound waves dissipate quickly with the distance from the propeller. At the same time, even when using a compressible flow formulation, the required fineness of computation mesh makes the direct far-field noise calculation practically unfeasible. For these reasons, the methods based on the acoustic analogy are commonly employed, where the sound sources obtained from the hydrodynamic solution are reduced to the emitters distributed over control surfaces, and the equations of the fluid motion in the far field are recast in the form of an inhomogeneous wave equation. The most common approach used with CFD solutions is based on the Ffowcs Williams-Hawkings (FWH) equations. It takes into account all fundamental noise sources – monopole (thickness of blades and cavities), dipole (blade loading), and quadrupole (non-linear contributions associated with turbulent structures, products of cavity destruction and vortex-vortex interaction in propeller slipstream). While the contributions from monopole and dipole sources are evaluated by computing surface integrals on the respective noise sources, the quadrupole term requires volume integration, which is very expensive since the whole solution field needs to be saved at every (and very small) time step. Therefore, instead the sound sources are evaluated on a permeable control surface which surrounds propeller and a "relevant" portion of propeller slipstream. In such formulations, for example Farassat Formulation 1A (Farassat, 2007), the terms responsible for monopole and dipole contributions lose their original strict meaning and become pseudo-monopole and pseudo-dipole terms, which include also the contribution from the quadrupole (non-linear) term, provided that the permeable control surface encompasses the whole turbulent wake, or at least a practically significant part of it. It has to be noted that the original FWH acoustic model is used only to predict sound propagation in free space. It does not account for the effects of reflection, refraction or material property change in the domain of receiver. These effects need to be modelled separately by, for example, mirroring the sources at the reflection surfaces and taking into account the acoustic properties of both materials at the interface. It thus becomes clear that should one aim at the prediction of noise radiated from the system propeller-rudder, the permeable control surface has to encompass the region of volume mesh around propeller and rudder. In presence of ship hull, whose boundary layer and wake are also the noise sources, an adequate choice of permeable surface becomes less obvious. All researchers who have used the FWH model with permeable surface in the acoustic calculation of propellers point out the importance of achieving an accurate, well-converged CFD solution for the hydrodynamic part. It necessitates a high-quality mesh to minimize numerical diffusion and adequate physics model to resolve propeller vortices and their cavitation.

In the present study, we investigated the possibilities of the Detached Eddy Simulation (DES) approach in combination with Adaptive Mesh Refinement (AMR) regarding the resolution of blade tip and hub vortices, propeller cavitation and its impact on integral characteristics. The benchmark case of PPTC propeller operating in straight flow was used as the test example (SMP'11, 2011). The commercial CFD code STAR-CCM+ (version 12.04) was employed.

2 Geometry and computation mesh

An accurate modelling of propeller blade geometry is important for producing a high-quality mesh, especially in the areas of blade leading and trailing edges and blade tip, where pressure gradients give rise to detached vortices. Upon the examination, it was found that the CAD files of PPTC propeller provided for the SMP'11 and SMP'15 Propeller Workshops reveal a number of issues related to surface quality in the aforementioned areas. For this reason, the blade geometry was regenerated from the original geometry tables given in PFF files, using the SINTEF Ocean in-house propeller design

software AKPA. The examples of comparison between the "old" and newly produced blade solid geometries are shown in Fig. 1. It can be seen that the surface quality in the areas of blade leading edge and tip is considerably improved in the new CAD model.

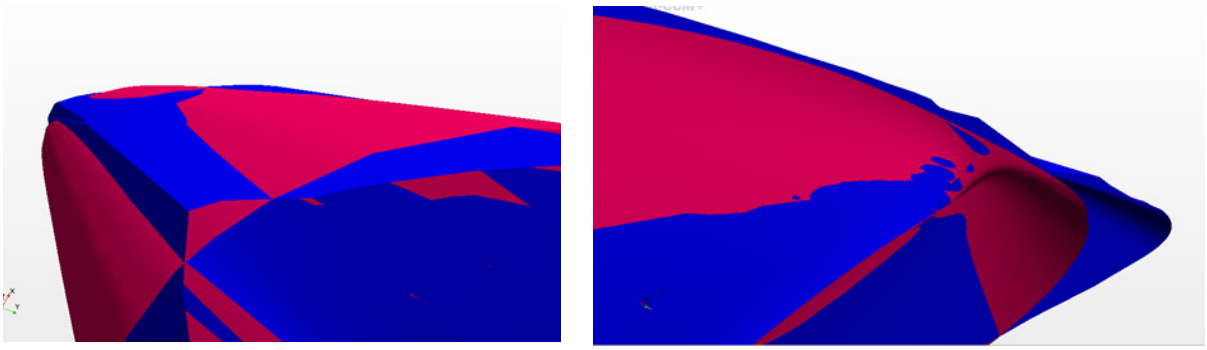

Fig.1: Comparison of PPTC propeller solid models (blue – old model provided to SMP Workshops, red – new model produced from the original PFF files).

The two configurations corresponding to open water tests in the towing tank and velocity field measurements and cavitation tests in the cavitation tunnel of SVA have been studied. The computation domain and propeller model for the second configuration are presented in Fig.2. The domain features the working section of the cavitation tunnel, extended to 15D (D – propeller diameter) towards the Outlet, and a long rotating propeller region (radius 0.6D, upstream interface 0.4D, downstream interface 2.0D). A long propeller region is used to avoid the diffusion of vortices near the propeller caused by the downstream interface, and to ensure that the zones of AMR, which are used for the resolution of the tip vortex, follow propeller rotation. The propeller model features the gap between the rotating hub and stationary dynamometer shaft, with the inner propeller shaft also included. This is done to provide as close as possible comparison with the test setup.

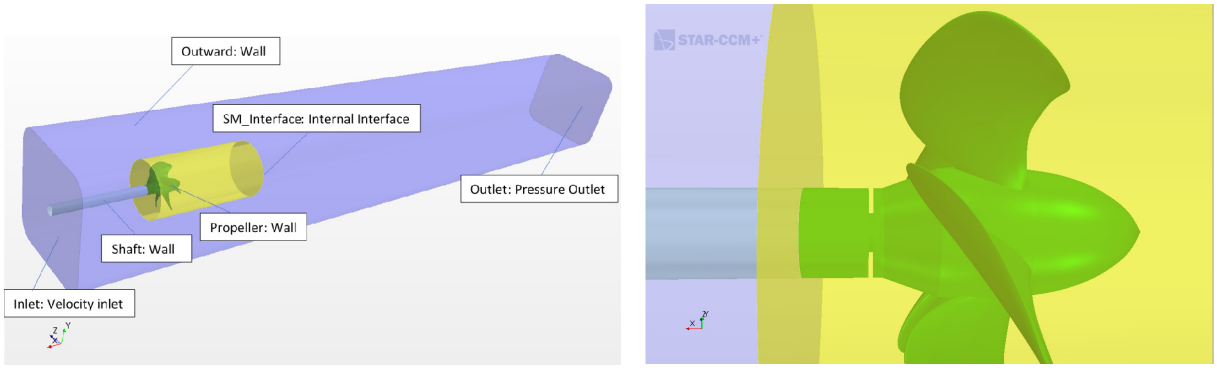

Fig.2: Computation domain and propeller model used in the simulations of velocity field measurements and cavitation tests in the cavitation tunnel

At this stage, the Sliding Mesh (SM) method is used to solve the motion of propeller region. The use of this method would be problematic in the case of propeller with rudder. Therefore, a more general solution based on the overset mesh technique is currently being developed.

The domain of outer fluid is represented by a hex-dominant trimmer mesh. For the propeller region, the two mesh types were investigated – the trimmer and polyhedral meshes. A systematic grid sensitivity study was conducted with both mesh types. For the configuration of cavitation tunnel tests, the results in terms of propeller thrust and torque coefficients (KTP, KQP) are presented in Table 1.

Table 1: Results of mesh sensitivity study with preliminary (non-AMR) meshes. Cavitation tunnel tests, J=1.253, n=23 (Hz). RANS, kwSST w/o transition.

Mesh	Refinement factor	No. of cells Total (mil)	Cell size on LE, %D	Cell size in slipstream, %D	KTP	KQP
Trim-3	k=1.25	13.8	0.0390625	1.25	0.2505	0.07297
Trim-2	k=1.00	21.6	0.03125	1.00	0.2490	0.07236
Trim-1	k=0.75	40.7	0.0234375	0.75	0.02495	0.07235
Poly-3	k=1.25	13	0.0390625	1.25	0.2522	0.07340
Poly-2	k=1.00	20.6	0.03125	1.00	0.2515	0.07358
Poly-1	k=0.75	40	0.0234375	0.75	0.2525	0.07343
Experimental values					**0.250**	**0.0725**

The preliminary meshes without AMR were used in this study. The refinement was done by varying the global mesh refinement factor applied to the mesh Base Size. Since all surface and volume cell sizes were set as values relative to the Base Size, they varied accordingly with the exception of first near-near wall cell height, which was kept constant to maintain the same wall Y+ values for all meshes (in this case, Y+ varied between 0.5 and 1.5 over propeller blade, the mean value being around 1.0). The RANS method with the k-w SST turbulence model without transition was used. The propeller KTP and KQP show little sensitivity to mesh refinement, since in the important areas, such as blade leading edge, the mesh is sufficiently fine. Even with coarser meshes the predicted values agree well with the experimental values. While, the polyhedral meshes allow in general a better approximation of propeller blade geometry, higher cell connectivity of polyhedral cells comes at the penalty of longer mesh generation time, larger storage needs, and longer computation time. Since for the resolution of tip vortices very fine meshes are needed, and since the AMR procedure may need to be applied several times during the solution, the trimmer approach has clear benefits. The computed velocity field in the propeller slipstream reveals a stronger dependency on mesh resolution. Fig.3 presents the computed fields of the axial velocity at the slipstream section x/D=–0.2 downstream of propeller plane, around the tip vortex core. The numerical results obtained on different meshes are compared with the LDV measurements. It can be noticed that finer meshes allow for a better resolution of flow features, but none of the RANS solutions on the preliminary meshes provides satisfactory details of the vortex in question. The solution on the polyhedral mesh (Poly-1) offers a better resolution compared to the solution on the trimmer mesh with similar refinement (Trim-1).

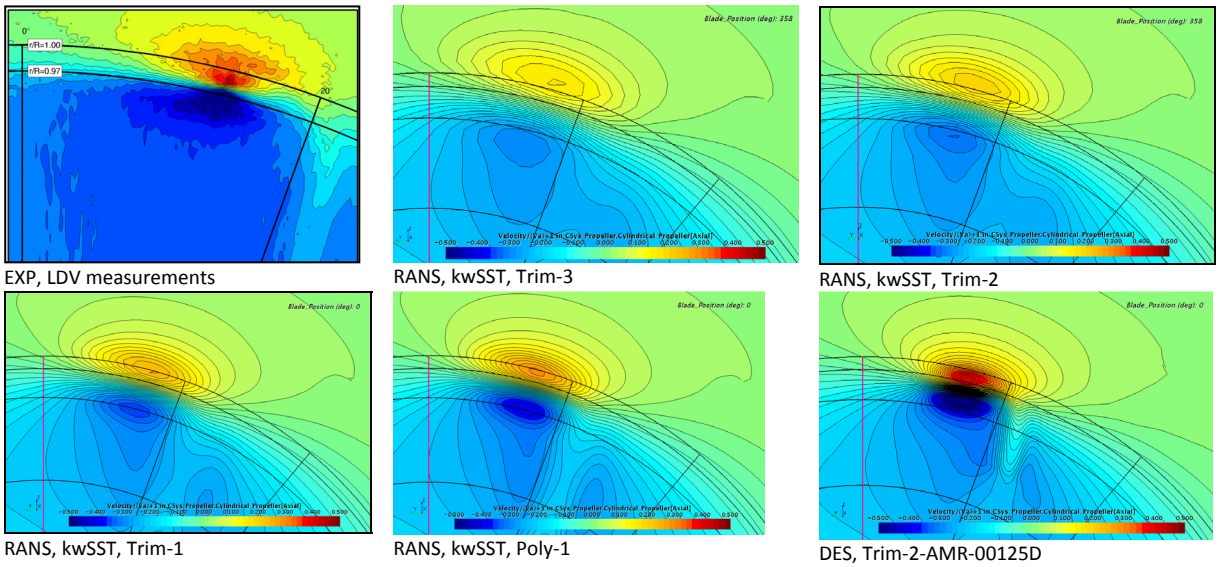

Fig.3: Field of the axial velocity at the slipstream section x/D=–0.2 in the tip vortex area. Cavitation tunnel tests, J=1.253, n=23 (Hz).

The computational effort associated with the mesh Poly-1 is however already quite heavy. Thus, a finer mesh in the area of the tip vortex and a more advanced turbulence modelling approach are required.

In order to address the problem of local mesh refinement, the AMR procedure was adopted using the Field Function Refinement Table applied in the propeller region. The field function uses Vorticity Magnitude as the AMR criterion, and it requires the desired fine cell size in the areas around the tip vortices where the vorticity magnitude is greater than the given user-specified value. Additional field functions are used to set geometrical constraints to limit the AMR procedure only to the tip vortex area. The AMR calculation workflow implies a preliminary calculation on the initial (non-AMR) mesh where the tip vortex area is modestly refined using a conventional volumetric control in the form of a subtracted cylinder. The cell size in the said volumetric control is 0.5% of D, which in the present case results in the total cell count about 20 mil. Depending on loading conditions, about 10÷15 complete propeller revolutions are performed to ensure a converged solution for the vorticity field in propeller slipstream. The computed field of vorticity is used as input to the AMR field function. The choice of appropriate cell size in the tip and hub vortex areas is not a trivial task. With scale resolving simulation in mind, one is usually guided by the consideration of scale of turbulent eddies one aims to resolve. The problem is however complicated by the fact that the flows we are studying may bear the features of both the globally unstable and locally unstable flows as per classification given in (Menter, 2015). For globally unstable flows, the recommended resolution, Δ_{MAX}, is of order of

$$\Delta_{MAX} \leq (0.05 \div 0.1) \cdot d_{REF} , \tag{1}$$

where d_{REF} is the characteristic diameter (e.g. hub diameter of tip vortex diameter). It results in 10 to 20 cells across the flow region of interest. For locally unstable flows, the overall recommendation is that the grid spacing should be sufficiently small to capture the initial flow instability of the separated boundary layer (e.g. in the area of tip vortex formation). Obviously, in the case of propeller, it would strongly depend on loading condition. The main relevant quantity to assess is the ratio between the grid length scale (grid spacing, Δ_{MAX}), and Turbulent Integral Length Scale, L_T. The latter quantity can be estimated from a precursor RANS calculation based on the Time Scale, τ, and Turbulent Kinetic Energy, k:

$$L_T = \tau \cdot k^{1/2} . \tag{2}$$

The cell size defining mesh resolution is then given by the formula

$$\Delta_{MAX} = R_L \cdot L_T , \tag{3}$$

where the aforementioned ratio R_L equal to 0.1 is commonly advised (Menter, 2015). Separately, one can check the estimation of grid spacing against the estimation of Taylor's microscale length (so-called inertial subrange where fluid viscosity significantly affects the dynamics of larger eddies of L_T scale):

$$\lambda_T = (10 \cdot k \cdot \nu / \varepsilon)^{1/2} . \tag{4}$$

Considering cavitating flows, one also needs to relate the cell size to the size of relevant cavitation structures. According to the experimental investigations presented in (Kuiper, 1981), the minimum radius of cavitation bubbles in the tip vortex of a 250 (mm) propeller model is found to be about 0.25 (mm), i.e. 0.1% of D. The use of prolonged cells (aspect ratio over 4.0) in the scale resolving mesh zones should be avoided to prevent vortex distortion and premature diffusion. Using isotropic (in the case of trimmer, cubic) cells is the best option. Different estimations of cell size required in the tip vortex area when using scale resolving simulations are presented in Table 2 for the test case studied in the present section.

Table 2: Estimation of cell size in the tip vortex area. Cavitation tunnel tests, J=1.253, n=23 (Hz).

Eq.(1), coeff=0.05	Eq.(3) – R_L=0.1	Eq.(4)	Size of cavitation bubbles
0.0013D	0.0010D	0.0012D	0.0010D

The example of AMR mesh produced with the cell size of 0.125% of D in the tip vortex and 0.25% of D in the hub vortex is shown in Fig. 4. The AMR is applied only within the rotating propeller region. Without the refinement around hub vortex, the total cell count is about 60 mil, while with hub vortex refinement included it is about 85 mil.

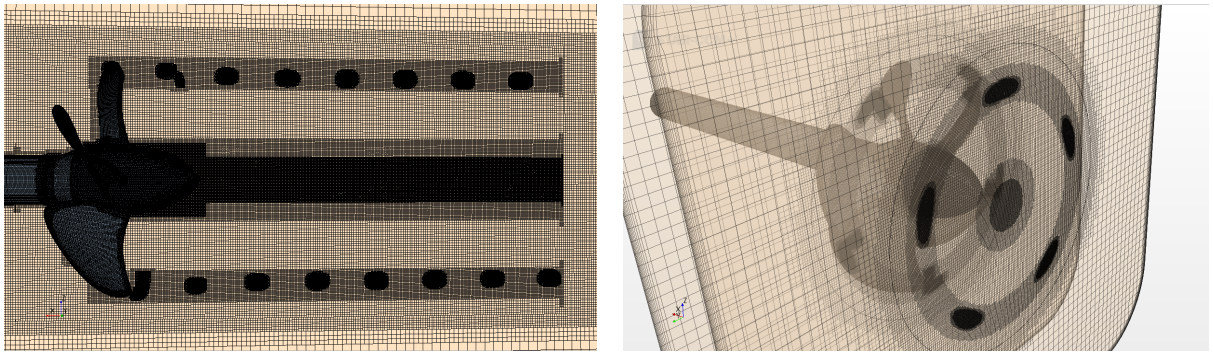

Fig.4: AMR mesh with refinement applied in the tip vortex and hub vortex areas.

The AMR procedure is found to have almost no influence on the prediction of integral propeller characteristics. The calculation on the AMR mesh can be started with the solution interpolated from the initial calculation on a non-AMR mesh, or directly from initial conditions. As regards the computation effort, there are no big differences between these two approaches. Similar to the case of initial mesh, about 10 to 15 propeller revolutions are needed to attain a converged solution. In the case of propeller in open water, straight flow conditions, one AMR update is sufficient.

3 Physics models

For scale resolving simulations, the IDDES method implemented in STAR-CCM+ is employed. In this method, the RANS zones are modelled using the k-w SST turbulence model with All Y+ Treatment algorithm at the wall boundaries. The DDES method introduces a delay factor that enhances the ability of the model to distinguish between the LES and RANS regions on meshes where spatial refinement could lead to ambiguous behaviour. Further, in the improved (IDDES) formulation, the sub-grid length-scale includes a dependence on the wall distance. This approach allows RANS to be used in a much thinner near-wall region, thus providing some wall-modelled LES capabilities. A hybrid 2nd-order upwind/bounded-CDS scheme is used for modelling the convection terms. As it can be concluded from the comparison in Fig. 3, the DES method applied in combination with AMR allows for a considerably better resolution of flow details in the tip vortex area, bringing the results closer to the experimental data. A comparison between the measured and computed velocity distributions along the radial station 1.0R, at the same slipstream section x/D=–0.2, is illustrated in Fig. 5. With the DES method, tracking of the blade tip vortex far downstream is possible, provided sufficient mesh resolution in the areas of interest.

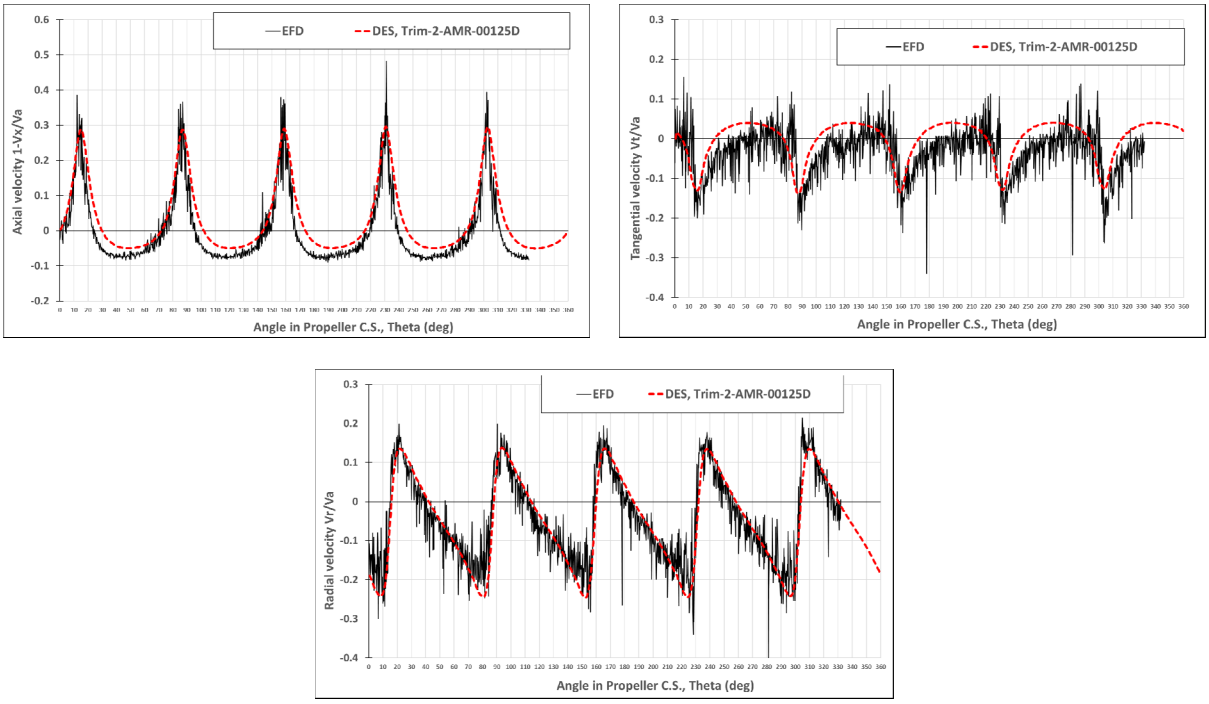

Fig.5: Distributions of velocity components along the radius 1.0R at the slipstream section x/D=–0.2. Cavitation tunnel tests, J=1.253, n=23 (Hz).

As far as the prediction of propeller forces is concerned, the results obtained with the DES and RANS method are found to be very close. The differences in computed thrust coefficient, KTP, were only within (0.5÷1.0)%, in the case of fully turbulent solution, and within (1.0÷1.5)% in the case of solution with the Gamma-Re-Theta transition model, the DES method showing lower values. The differences in torque coefficient are even smaller.

For the modelling of propeller cavitation, the Eulerian Multiphase model was employed with the VOF method. The Scherr-Sauer (SS) cavitation model was used, which is based on the asymptotic form of the Reyleigh-Plesset equation where the effects related to bubble dynamics, viscous diffusion and surface tension are neglected. To have a rough control over the bubble growth rates, the implementation of the SS model in STAR-CCM+ provides the two so-called scaling factors that may be used to increase/decrease bubble production and accelerate/decelerate their collapse. The default values of bubble Seed Density (10^-12 (1/m^3)) and Seed Diameter (10^-6 (m)) were assumed. In the VOF solution, the 2nd order discretization scheme was used, with the default values of the Sharpening Factor (0.0), Angle Factor (0.5), CFL_l (0.5) and CFL_u (1.0).

To test the performance of the method in the case of cavitating flow, the two test conditions of the PPTC propeller were investigated: (J=1.269, σn=1.424) and (J=1.019, σn=2.024). The simulation workflow followed the AMR procedure described above. After the converged AMR solution for fully wetted flow was attained, the cavitation model was enabled. The desired cavitation number is achieved by providing the corresponding Reference Pressure at the given Saturation Pressure of water. During the first propeller revolution of the cavitating flow stage, the Reference Pressure is gradually reduced from the atmospheric value to the value of cavitating pressure. The DES method was used from the beginning of simulation, in both the initial and AMR meshes. The time step corresponded to 2 (deg) of propeller rotation at non-cavitating calculation stages, and it was reduced to 1 (deg) at the stage of cavitating flow. 5 inner iterations per time step were allowed. The time step of 1 (deg) used at the final cavitating flow stage resulted in CFL values about 1.0 in most of the slipstream region, and

about 10.0 in the AMR regions around tip vortices. In order to provide CFL=1.0 in the AMR regions, the time step of 0.1 (deg) would be required, which makes the numerical solution very expensive. Variation of time step between 2 and 0.5 (deg) did not lead to noticeable changes in the results.

The time histories of computed propeller thrust coefficient and cavitation volume are presented, for the two investigated conditions, in Fig. 6. For the condition of lighter propeller loading, J=1.268, the solution convergence can be judged quite good. However, at the condition of heavier loading, J=1.019, a converged solution was not achieved. Such solution behaviour was caused by the reflection of pressure waves from the Pressure Outlet boundary. In the case of heavier loading (and more intensive cavitation), the production of vapour in the beginning of simulation resulted in a strong pressure wave travelling through the confined domain of cavitation tunnel and reflecting from the outlet. This phenomenon is greatly reduced, and eventually vanishes, when the dimensions of computation domain are increased in Y-Z-directions, i.e. when the setup gets closer to open water conditions. The use of non-reflecting outlet boundary conditions may be one possible remedy to this situation. However, since a high-quality hydrodynamic solution is of paramount importance for the prediction of pressure pulses and noise, modelling the whole cavitation tunnel domain may be the only viable alternative when simulating the setup of cavitation tests. In such a setup, a pressure chamber with free water surface needs to be included, as in the testing facility, which would absorb the aforementioned pressure waves. The flow in the cavitation tunnel would be driven by an actuator disk – an additional region, where the axial momentum sources are adjusted to provide the desired flow speed in the tunnel working section.

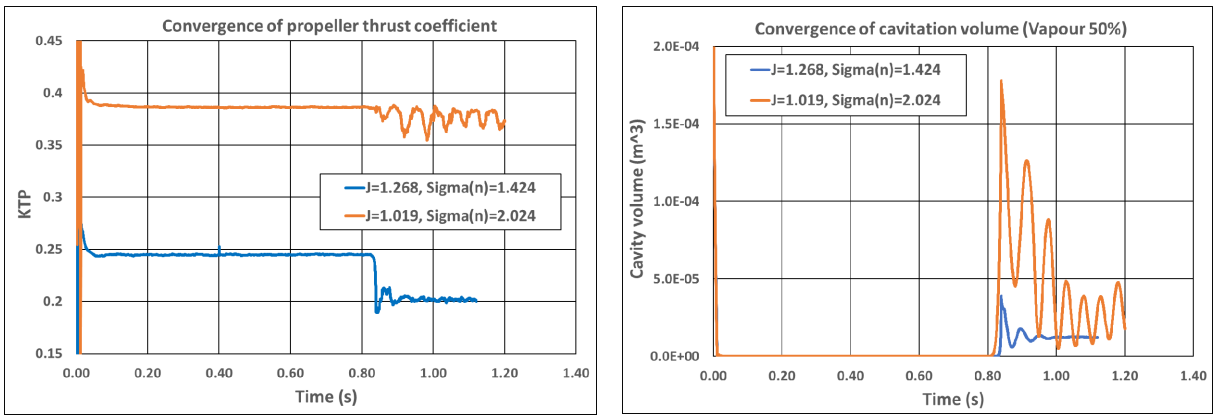

Fig.6: Convergence of propeller thrust and cavitation volume at the two test conditions. n=25 (Hz), Pv=2818 (Pa).

A comparison between the measured and computed mean values of propeller thrust and torque without and with cavitation is presented in Table 3. From this comparison it can be concluded that the numerical method reflects adequately the influence of cavitation on the mean integral characteristic of propeller. A comparison between the experimental observations and predictions of cavitation patterns is illustrated in Fig.7 and 8. The predicted extents of cavitation on the suction and pressure side of the blade are found to be in a satisfactory agreement with experimental observations. A larger extent of cavitation predicted along the leading edge on the suction side of the blade at the condition (J=1.019, σn=2.024) has earlier been noticed by other authors, and so far has not received a plausible explanation, other than possible local deviations between the blade geometries used in numerical simulations and physical tests. The resolution of cavitating tip vortex achieved with the DES method using the AMR approach is considerably better compared to that achievable with the RANS method. However, cavitation in the tip vortex is not predicted as far downstream as it is observed from model

tests, in particular in the case of lighter loading where the tip vortex is weaker. An even finer mesh resolution may be needed in such cases as well as further improvements in the cavitation model. The prediction of tip vortex strength and cavitation depending on blade loading requires closer investigations. The occurrence and extent of hub vortex cavitation is generally reproduced well by the calculations.

Table 3. Influence of cavitation on integral propeller characteristics.

	EXPERIMENT		CFD	
	KTP	**KQP**	**KTP**	**KQP**
J=1.268				
Atm	0.245		0.245	0.07054
Cav, σn=1.424	0.2064	0.06312	0.2016	0.06270
J=1.019				
Atm	0.387		0.3860	0.09940
Cav, σn=2.024	0.3735	0.09698	0.375	0.09680

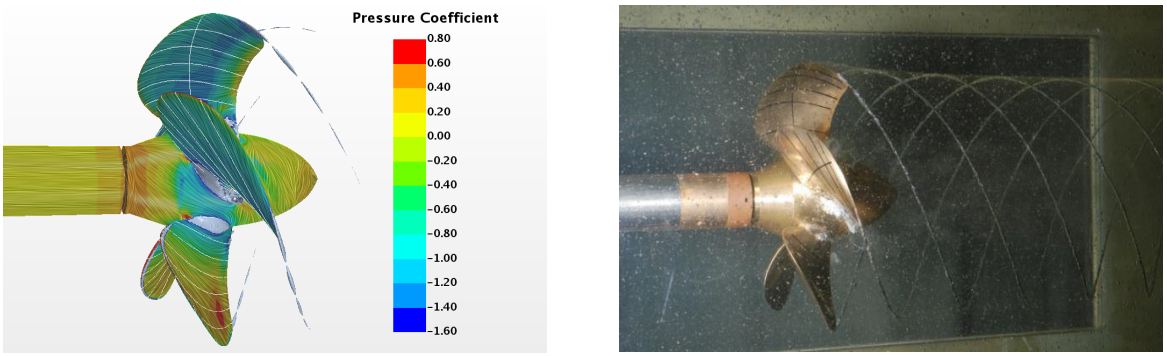

CFD (cav. tunnel domain) Experiment, cav. tunnel

Fig. 7: Computed and observed patterns of cavitation. J=1.268, σn=1.424

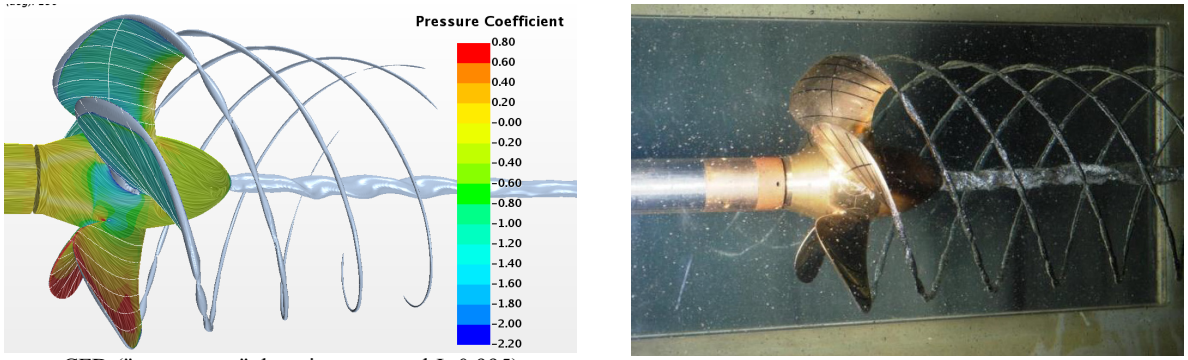

CFD ("open water" domain, corrected J=0.995) Experiment, cav. tunnel

Fig. 8: Computed and observed patterns of cavitation. J=1.019, σn=2.024

4 Conclusions

Scale resolving simulations such as the IDDES method applied in the present work demonstrate clear advantages over traditional RANS approaches in the resolution of propeller tip and hub vorticity, which is essential for the prediction of propeller induced pressure pulses and noise. Due to a very fine mesh required in the tip vortex area, the use of conventional pre-defined volumetric controls results in extremely high cell counts that render simulation impractical. Therefore, the use of Adaptive Mesh Refinement (AMR) procedure based on the vorticity magnitude (or equivalent) criterion appears a

plausible alternative. The numerical method shows satisfactory agreement with experimental data on the PPTC propeller regarding the integral propeller characteristics, velocity field in the tip vortex area, and cavitation patterns. As regards the comparison with model tests done in the cavitation tunnel, one of the major challenges is related to the problem of non-physical reflection of pressure waves from the outlet boundary, especially pronounced at heavier loading of propeller where cavitation is more intensive. The preferred approach to deal with this problem is to simulate the whole domain of cavitation tunnel with pressure chamber. However, alternative artificial measures are also worth investigating.

Acknowledgements
The author acknowledges the support and funding by the MarTERA ERA-NET program, represented by BMWi-project (03SX461C) “ProNoVi” for the German partners (TUHH, Fr. Lürssen Werft GmbH & Co. KG, SCHOTTEL GmbH), the Research Council of Norway Project 284501 for the Norwegian Partners (SINTEF Ocean, Helseth AS) and MIUR-project “ProNoVi” for the Italian partners (CNR-INM).

References

Bensow, R. & Liefvendahl, M. (2016): "An acoustic analogy and scale-resolving flow simulation methodology for the prediction of propeller radiated noise." 31st Symposium on Naval Hydrodynamics, Monterey.

Farassat, F. (2007): “Derivation of formulations 1 and 1A of Farassat.” Technical Memorandum TM-2007-214853, NASA, NASA Langley Research Center (USA).

Felli M, Grizzi S, Falchi M. (2014): "A novel approach for the isolation of the sound and pseudo-sound contributions from near-field pressure fluctuation measurements: analysis of the hydroacoustic and hydrodynamic perturbation in a propeller-rudder system." Experiments in Fluids. 2014;55–1(1651).

Kuiper, G. (1981): "Cavitation Inception on Ship Propeller Models." Wageningen.

Menter, F.R. (2015): "Best Practice: Scale-Resolving Simulations in ANSYS CFD." Version 2.00 ANSYS Germany GmbH, November.

Muzaferija, S., Papoulias, D., Peric, M. (2017): "VOF Simulations of hydrodynamic cavitation using the asymptotic and classical Rayleigh-Plesset models." Fifth International Symposium on Marine Propulsors, Espoo, Finland, June 12-15.

Shin, K.W & Andersen, P. (2018): "CFD Analysis of Propeller Tip Vortex Cavitation in Ship Wake Fields." Proceedings of the 10th International Symposium on Cavitation (CAV2018), Baltimore, USA.

SMP'11 (2011): "Potsdam Propeller Test Case (PPTC). Cavitation Tests with the Model Propeller VP1304, Case 2.3", Second International Symposium on Marine Propulsors SMP'11, Workshop: Propeller performance, Potsdam, May.